Atmospheric Effects on Long Stand-Off HSI Applications

Dr. A.D. Cropper and Dr. David C. Mann
Raytheon Company
2501 W. University Dr.
McKinney, TX 75071
UNITED STATES OF AMERICA

A.D.Cropper@raytheon.com

ABSTRACT

Hyperspectral Imaging (HSI) is finding utility in many new areas, such as environmental and agricultural monitoring, medicine and food technology, industrial inspection, land management, and defense usage, due to its ability to simultaneously collect both spatial and spectral information. Within the tropical environment the utility of HSI has been demonstrated through various rain forest and coastal environmental programs.

System performance for all HSI systems is influenced by many factors, including environmental conditions, operational usage, internal system composition and the processing chain. Truly optimizing this performance requires an understanding of the operational conditions under which each system will perform. One of the key factors affecting system performance, especially at long stand-off ranges, is the atmospheric effects. This paper presents analytical results from the visible to long wave infrared demonstrating the effects of atmospheric conditions on long stand-off airborne HSI systems based on a Raytheon developed performance model for estimating System performance.

This end-to-end System Performance Model is especially designed for long stand-off airborne detection with large off-nadir viewing angles. It takes into account most of the components within the entire imaging chain. The model divides the end-to-end imaging chain into three parts: the environmental component, the Concept of Operations (CONOPS), and the imaging system effects. The environmental component includes solar illumination, scattering, and atmospheric transmittance. The system component includes the effects of system noise and throughput. The CONOPS accounts for the various operating conditions best suited for long stand-off detection. The Dual Band analytical results presented in this paper provide details on the influence of the atmospheric conditions, including tropical conditions, on NESR and SNR performance in a Spot Mode CONOPS for a HSI system based on the end-to-end System Performance Model.

INTRODUCTION

Hyperspectral imaging has been used for Remote Sensing in environmental, military, civilian and scientific applications [1, 2, 3, 4]. Physics based models have been developed [5, 6, 7, 8] to better understand the performance of these HSI systems. This paper is devoted specifically to results related to atmospheric effects on solar reflected and emissive long stand-off airborne HSI systems based on a Raytheon developed performance model for large off-nadir viewing angles.

This paper reports on the application of the Raytheon System Performance Model (hereinafter, the Model) [9] to understanding the effects of atmospheric conditions on system performance using two scenarios, a scene comprised of a single reflective target (scenario 1) and scene comprised of a mixed reflective target (scenario 2) at 50kft altitude with off-nadir viewing angles of 80° and 65°.

Under scenario 1 the Model specifically looks at the effect atmospheric conditions have on large off-nadir viewing angles using a scene comprised of a single 25% and 50% reflective target. In scenario 2 the Model then applied the most favorable atmospheric conditions to collecting against a mixed scene comprised of an olive green target within mixed forest background.

The COTS-like NIR/SWIR Concept System used within the Model consisted of a turret, NIR/SWIR Camera, and Imaging Spectrometer. A representative LWIR HSI system is also modelled in Scenario 2.The Model assessed the atmospheric effects on two key performance parameters (KPPs): Noise Equivalent Spectral Radiance (NESR) and Signal-to-Noise Ratio (SNR) at altitudes of 50kft above ground level (AGL).

BACKGROUND

Hyperspectral imagery contains both spatial and spectral information about a target of interest within the scene. This information is disturbed by the spectral properties of the atmosphere, illumination, and the environment, as well as the internal system noise. With this Model we aim to develop a tool that provides insight into the sensitivities and significance of the various system parameters in achieving mission performance, similar to those developed by other physics-based system models [10, 11].

The end-to-end model includes all the elements of the scene, such as the illumination, surface and atmospheric effects and the sensor's spatial, spectral and radiometric effects. The Model is driven by a set of input parameters that describe the scene, atmospheric conditions, sensor characteristics and the CONOPS. These parameters are used to transform the spectral reflectance or emittance through the spectrometer imaging chain. The spectral conditions are propagated from reflectance or emittance to spectral radiance to sensor signals that are then use to create metrics of system performance.

The Model in scenario 2 considers a scene comprised of a target and a mixed background. It assumes that the target size is sub-pixel and the remainder of the pixel is filled with a mixed background. It should be noted that this model does not account for a specific spatial layout, but rather takes into account a target immersed in a mixed background. A simple linear model is assumed for the target and background combination, where the parts of each add up to 100% of a pixel.

The target and background spectral reflectance and emittance components, assumed to come from diffuse surfaces, are created elsewhere and are provided as inputs to the Model. The Model uses the MODTRAN5 code to compute the solar illumination and atmospheric effects. The total radiance arriving at the sensor consists of direct and diffused light. The model used here has been developed for sensor systems operating in the reflected and emissive portions of the optical spectrum, with scenes near room temperature.

This Model can be used to determine any influence atmospheric conditions have on large off-nadir viewing angle Missions. In scenario one, the effects of atmosphere were evaluated against a 25% and 50% reflective Target. Then in scenario two, the Model applied a COTS-like NIR/SWIR Concept System collecting against an Olive Green target within mixed forest background to the most favorable atmospheric conditions. A Concept LWIR System is also applied to Scenario 2 using all atmospheric conditions to illustrate the deleterious effect of water vapor on long range LWIR HSI.

The Model evaluated the NESR and SNR as function of off-nadir viewing angles (80° and 65°) at altitudes of 50kft, with an aircraft speed of 100kts. The CONOPS of Altitude, Speed, and Viewing Angle, were traded in the Model for best results.

The stand-off CONOPS used within the Model for a side looking collection from a large off-nadir angle with a long slant range was the spot mode. Here, the turret back scanning mode partially compensates for the forward velocity of the aircraft, as well as providing line of sight (LOS) stabilization to the pushbroom collection. The collection rate (m/s) is equal to the aircraft ground speed minus the back scan velocity. Velocity smear is minimized but the coverage area is reduced. Note that the spot mode does not allow for continuous scanning, but can provide multiple spot collections during mission flights.

PERFORMANCE MODEL

This end-to-end System Performance Model [9] takes into account the environmental component, the CONOPS and the imaging system effects and is broken into inputs and outputs of the model. Inputs to the Model include the environmental component of the solar and thermal illumination, scattering, and atmospheric transmittance, as well as the system component (such as the effects of system noise and throughput), and the physical makeup of the sensor system.

The Key Output parameters reported within this paper are the NESR and SNR. For a spectral band with center wavelength λ, and signal spectral radiance $L_s(\boldsymbol{\lambda})$, the NESR is given by [12]:

$$NESR_{(\lambda)} \cong \frac{L_s(\lambda)}{SNR\ (\lambda)} \qquad (1)$$

The NESR units are given in micro-flicks (μf) or (μW/(cm^2·sr·μm)). The SNR for a band centered at λ can be derived from the total scene target radiance, $R_R(\boldsymbol{\lambda})$ and the total noise (N_{tot}) [12]:

$$SNR(\lambda) = \frac{R_R(\lambda)}{N_{tot}}. \qquad (2)$$

VNIR/SWIR REGION

The work and results are presented in two sections. This section covers the visible/near infrared/short wave infrared (VNIR/SWIR) results. The next section covers the long wave infrared (LWIR) results.

Atmospheric Effects

For long range imaging applications, the effects of atmosphere become extremely important. The atmosphere can be viewed as a spectral filter for light traveling from a target to the sensor. This light is scattered, absorbed and reflected by air molecules and aerosols. Thus light reaching the sensor is a combination of the light scattered from the Sun and other sources, and light that is reflected and emitted from Earth's surface. The spectral filter effect reduces the amount of light from the target that reaches the sensor, slightly reducing it at some wavelengths and completely eliminating it in others. Conversely, light emitted or scattered into the path creates a background glow that also varies spectrally. Both of these effects degrade imaging performance.

The MODTRAN5 radiative transfer program was used to model various atmospheric and scene scenarios to explore the effects of atmospherics on the two KPPs of a large off-nadir imaging system. The initial parameters

for our 50kft platform altitude included various LOS elevation angles, surface albedos, atmospheric models, and solar azimuth angles.

Four standard MODTRAN atmospheric models were examined during scenario one: Tropical, Mid-Latitude Summer, Mid-Latitude Winter, and Sub-Arctic Winter [14]. With scenario two, the report focuses on the Mid-Latitude Winter and Sub-Arctic Winter models, which provide the best imaging conditions due to the low water vapor content of these models.

Figure 1 illustrates the VNIR/SWIR spectral transmittance for the first scenario of a 25% and 50% reflective target at 50 kft. AGL altitude with 80° and 65° off-nadir viewing angle with two solar conditions, "0" which pertains to the sun in front of the aircraft and "180" when the sun is behind the aircraft.

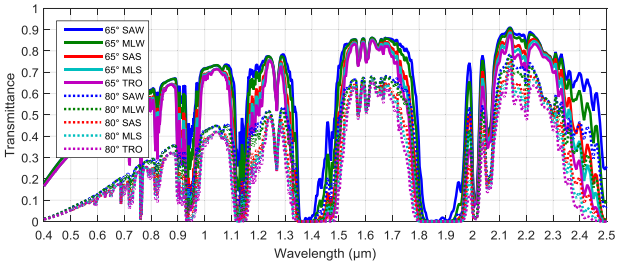

Figure 1: Spectral transmittance at 25% and 50% for 50kft AGL at 80° and 65° off-nadir viewing

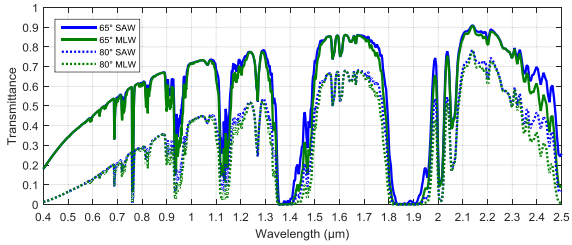

Figure 2: Scenario 2 MLW & SAW Spectral transmittance for 50kft AGL at 80° and 65° off-nadir

Figure 2 illustrates the VNIR/SWIR spectral transmittance for the scenario 2 using only the most favorable atmospheric conditions (MLW and SAW) at 50kft from a 65° and 80° off-nadir viewing angle.

In scenario 2, various combinations of target and background scene materials were modelled in MODTRAN. The goal of using these combinations in the Model was to allow the evaluation of atmospheric effects on a sub-pixel-sized target material in mixed background.

A feature of MODTRAN was exploited for this task, the ability to use different materials for the target pixel (from which light travels directly to the sensor system) and the area around the target pixel (from which light is scattered into the Sensor's LOS). Two cases were calculated for each target and background combination, one case with the target material in the target pixel, and the other with the background material in the target pixel (in both cases, the background material is used for the area around the target pixel).

Figure 3 illustrates the VNIR/SWIR spectral albedos of the materials used within the model for scenario 2. The albedos for conifer, deciduous, and grass are from the ASTER spectral library [15]. The first four materials in the legend are background materials and the last one is the target material. The olive green paint was used to represent the target immersed within a mixed forest background comprising of conifer, deciduous, and grass.

The target pixel and total spectral radiance curves as described above for SAW and MLW atmosphere conditions were used in the scenario 2 to evaluate the Concept System for NESR and SNR. Figure 4 illustrates the NIR/SWIR average total, target and mixed background spectral radiance for MLW and SAW atmospheres at 80° and 65° off-nadir angles, averaged over the different background vegetation (Scenario 2).

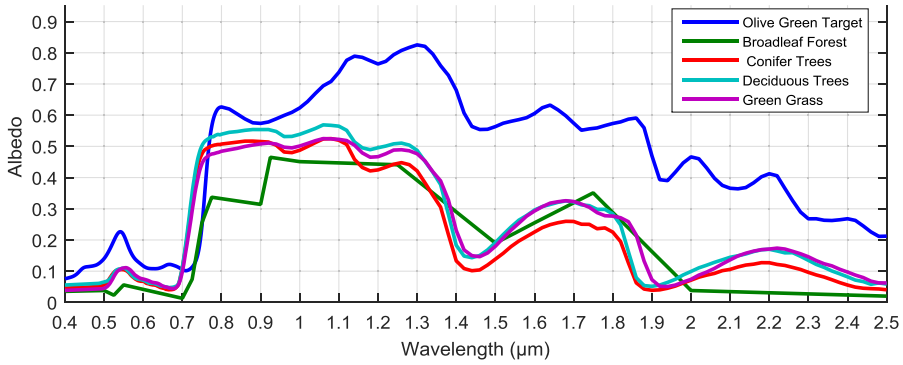

Figure 3: VNIR/SWIR Spectral albedos used in Model

In addition, Scenario 2 assumes that light from the surrounding material is scattered into the path contributing to the atmospheric background radiance.

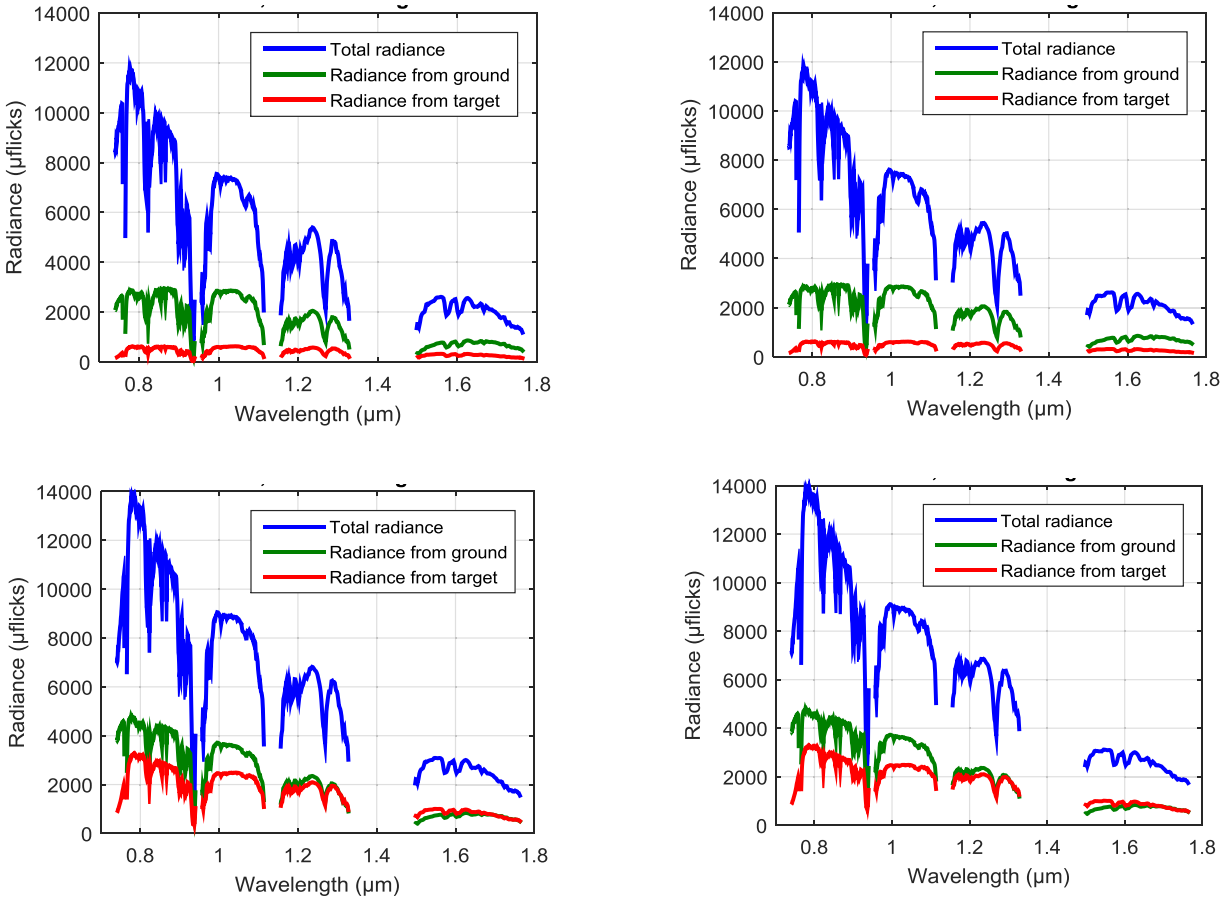

Figure 4: NIR/SWIR Average Spectral Radiance

As expected, the MODTRAN results show that the lower LOS elevation angle (which leads to a shorter slant range) and a higher surface albedo produce more favorable imaging conditions (higher scene radiance and lower background radiance at the aperture). Of the two solar positions examined (45° zenith angle, 0° or 180° azimuth angle relative to the LOS azimuth angle), putting the Sun behind the platform (180° relative azimuth angle) produced less background radiance; henceforth this placement is used in the second scenario analysis within the Model.

For Scenario 1 the Model analyzed a target with 25% and 50% reflectivity at 50 kft. altitude with 80° and 65° off-nadir viewing angle and two solar conditions, "0" (sun in-front of the sensor) and "180" (sun behind the sensor) for NESR and SNR. The target performance at 25% reflectivity was found to be significantly lower even at the most favorable atmospheric conditions. Thus only the target at 50% reflectivity results will be discussed within the remainder of the paper.

Figure 5 and Figure 6 show the NESR and SNR for the Mid-Latitude Winter (MLW) and Sub-Arctic Winter (SAW) conditions with the **Sun in-front** of the sensor at a 45° solar zenith and with a 65° and 80° off-nadir viewing angles at a frame rate of 30 Hz with 16 co-adds. The dashed black line indicates an example of a typical SNR specification at nadir and is included here for comparison. The SNR results at these atmospheric conditions were below the nadir specification of 200.

Figure 7 and Figure 8 show the NESR and SNR for the same Mid-Latitude Summer (MLS) and Tropical (TRO) conditions at 65° and 80° off-nadir viewing angles respectively. Again these atmospheric conditions produced similar results for SNR.

For the **Sun location behind** (180) the sensor at a 45° solar zenith, Figures 9, 10, 11 and 12 show the NESR and SNR for the MLW, SAW, MLS and TRO conditions with 65° and 80° off-nadir angles at a frame rate of 30 Hz with 16 co-adds respectively. The outcome from the initial analysis showed that the best performance occurred at MLW and SAW with the sun behind.

A key observation from the results was the narrowing of the profiles width with increasing moisture in the atmospheric conditions. For example, at a wavelength of 1 µm, the MLW performed best at 65° off-nadir viewing followed by the SAW, MLS and then TRO. For the 80° off nadir viewing the SAW was the best performer. This was then followed by the MLW, MLS and then TRO.

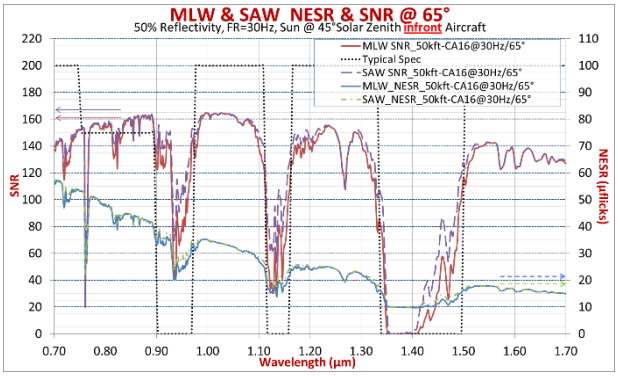

Figure 5: MLW and SAW NESR and SNR at 65°

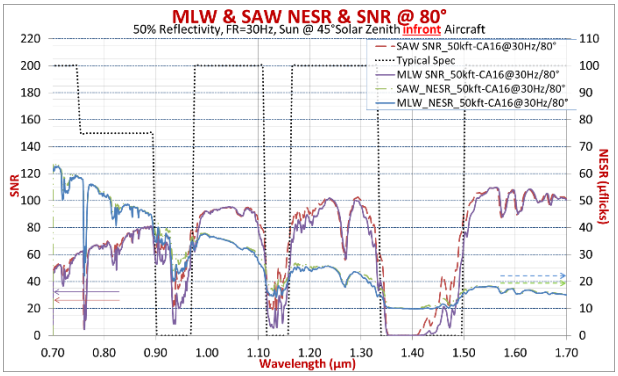

Figure 6: MLW and SAW NESR and SNR at 80°

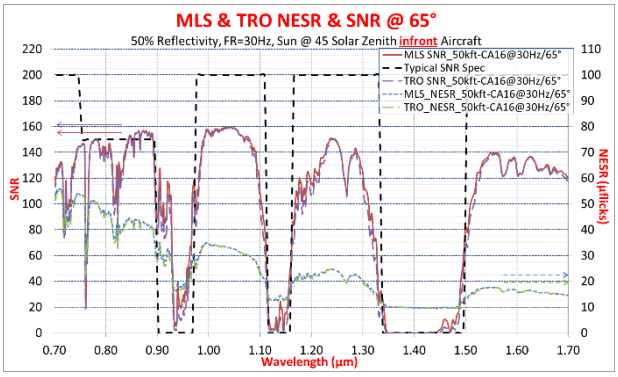

Figure 7: MLS and TRO NESR and SNR at 65°

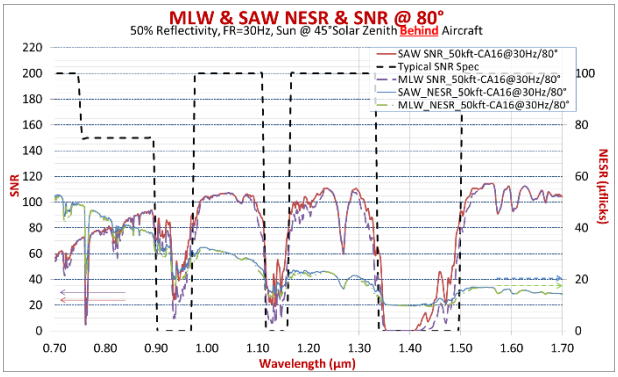

Figure 10: MLW and SAW Sun behind at 80°

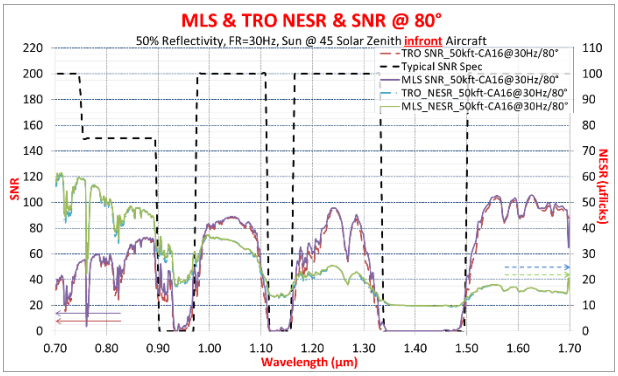

Figure 8: MLS and TRO NESR and SNR at 80°

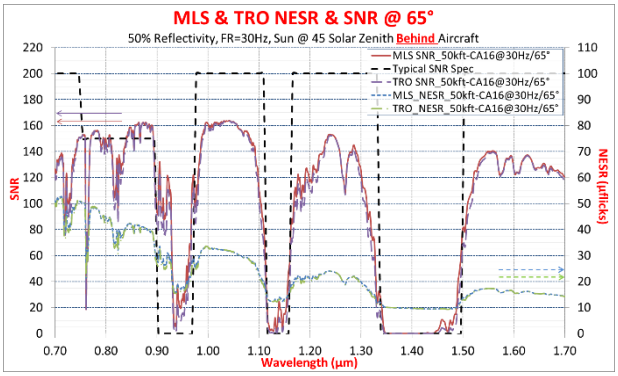

Figure 11: MLS and TRO Sun behind at 65°

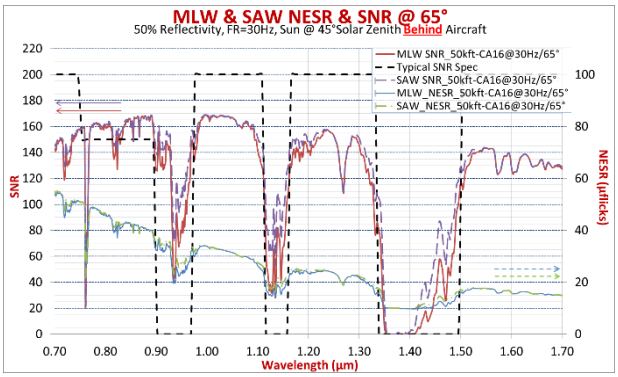

Figure 9: MLW and SAW Sun behind at 65°

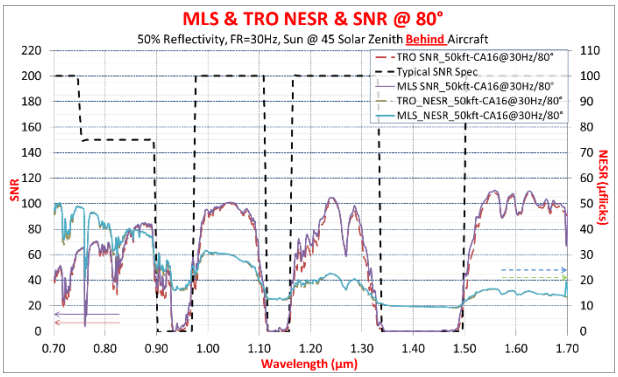

Figure 12: MLS and TRO Sun behind at 80°

The second scenario evaluated by the performance Model was the COTS-like NIR/SWIR concept system. The results when applied to an olive green target placed within a four-vegetation forest background under MLW and SAW atmospheric conditions at 50kft AGL altitudes at 60 and 30 Hz frame rate can be seen in Table 1.

Table 1: NIR/SWIR MLW & SAW Model Results, Scenario 2

Parameters	Scenario 2 (50,000ft; Sensor System Performance Results)							
CONOPS	80° Off Nadir; 60Hz; 1 co-adds; 50m/s Back Scan	80° Off Nadir; 30Hz; 1 co-adds; 50m/s Back Scan	80° Off Nadir; 60Hz; 4 co-adds; 50m/s Back Scan	80° Off Nadir; 30Hz; 4 co-adds; 50m/s Back Scan	65° Off Nadir; 60Hz; 1 co-adds; 50m/s Back Scan	65° Off Nadir; 30Hz; 1 co-adds; 50m/s Back Scan	65° Off Nadir; 60Hz; 4 co-adds; 50m/s Back Scan	65° Off Nadir; 30Hz; 4 co-adds; 50m/s Back Scan
Parameters	**Mid Latitude Winter Performance Results**							
$NESR_{(@1um\ in\ MLW/SB)}$ # (uf)	10.89	7.67	5.42	3.83	11.99	8.47	5.99	4.24
$SNR_{(@\ 1um\ in\ MLW/SB)}$ #	381.98	540.42	763.96	1080.84	590.53	835.41	1181.06	1670.82
Parameters	**Sub Arctic Winter Performance Results**							
$NESR_{(@1um\ in\ SAW/SB)}$ # (uf)	10.91	7.71	5.46	3.86	12.03	8.50	6.02	4.25
$SNR_{(@\ 1um\ in\ SAW/SB)}$ #	383.11	542.01	766.21	1084.02	591.68	837.04	1183.36	1674.08

The performance results for the MLW and SAW atmospheric conditions were quite similar. The former showed slightly better performance for NESR and the latter performed better with SNR. The NESR, and SNR performance results for both the MLW and SAW atmospheric conditions at 50kft occurred at a 65° off-nadir viewing angle, with a 30 Hz frame rate and 4 co-adds.

The Scenario 2 NIR/SWIR plots of NESR and SNR as a function of wavelength can be seen in Figure 13 and Figure 14 for the MLW and SAW atmospheric conditions at 50kft AGL altitude for 65° and 80° from 0.7µm to 1.7µm wavelength range.

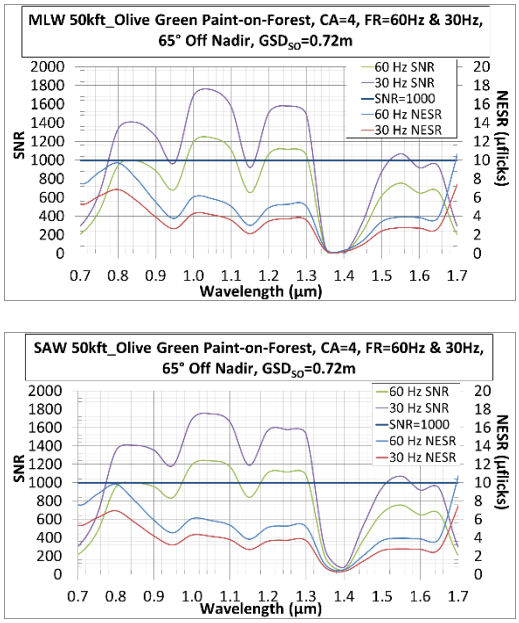

Figure 13: MLW and SAW Results at 65°

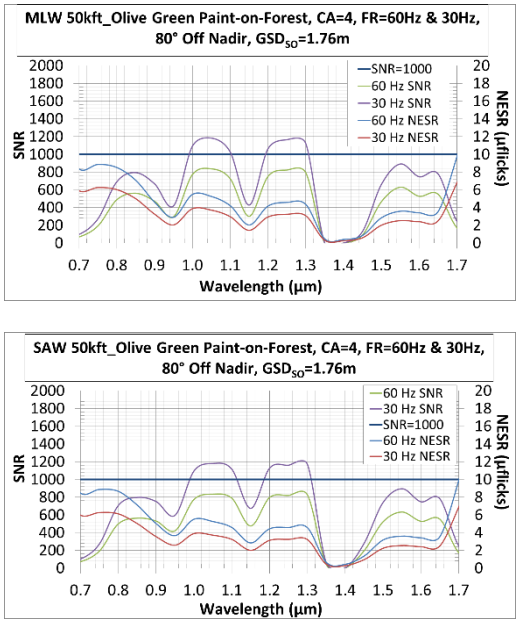

Figure 14: MLW and SAW Results at 80°

LWIR REGION

A model of a conceptual LWIR HSI system was applied to Scenario 2, using all four atmospheric conditions. This was done to illustrate the severe effect that water vapor has on LWIR HSI. As in the VNIR/SWIR case above, the SNR and NESR results are meant to illustrate the differences among different atmospheres and slant ranges.

Atmospheric Effects

Figure 15 illustrates the spectral albedo of the modelled materials in the LWIR band and the transmittance of the various atmospheric paths. Because there is such a drastic variation in transmittance for different atmospheres, a more detailed study was done with MODTRAN. Figure 16 illustrates the results of this study, showing that water vapor reduces atmospheric transmittance in the more difficult atmospheres (TRO and MLS (MLS results not shown)). The transmittance effect of water is broken up into two components in MODTRAN, including band absorption/scattering and continuum absorption/scattering. The figure illustrates the effects of other significant components, but these do not change very much among the different atmospheres.

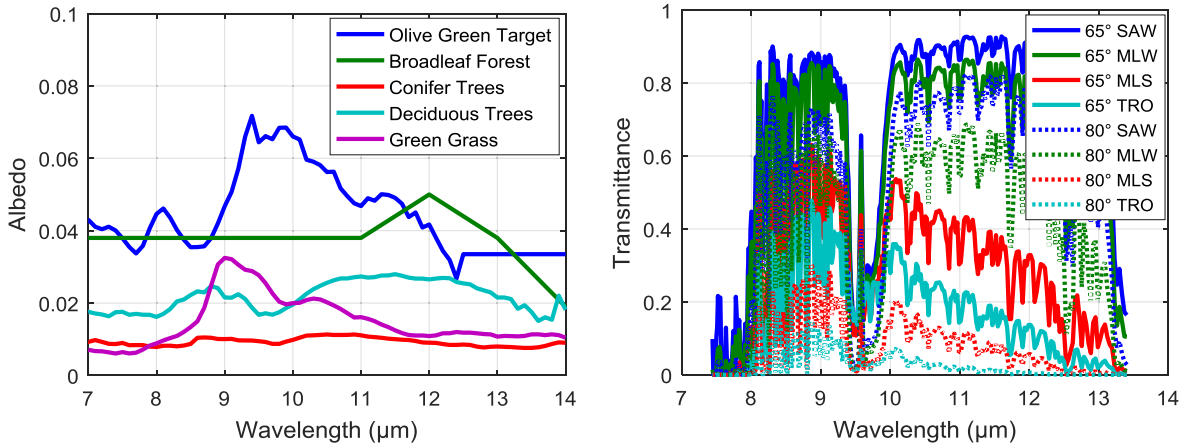

Figure 15: Spectral albedo of ground and target materials (left); Spectral transmittance of the various atmospheric paths (right).

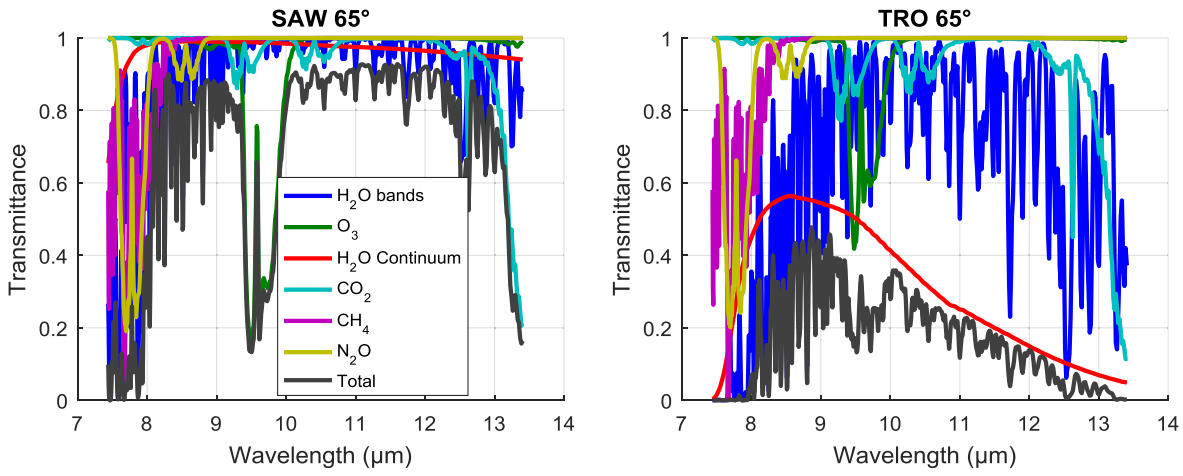

Figure 16: Contributions to atmospheric transmittance for SAW, 65° off nadir (left), and TRO, 65° off nadir (right). The "Total" curves include the effects of all atmospheric components, not just the ones illustrated here.

Figure 17 illustrates some examples of at-aperture radiance values. Like the similar NIR/SWIR results, these results were calculated with a subpixel target. Despite receiving similar total radiance at aperture between SAW and TRO atmospheres, the direct radiance from the ground, and the target in particular, is much lower in the TRO atmosphere than the SAW atmosphere. This has significant implications for system performance, as shown below.

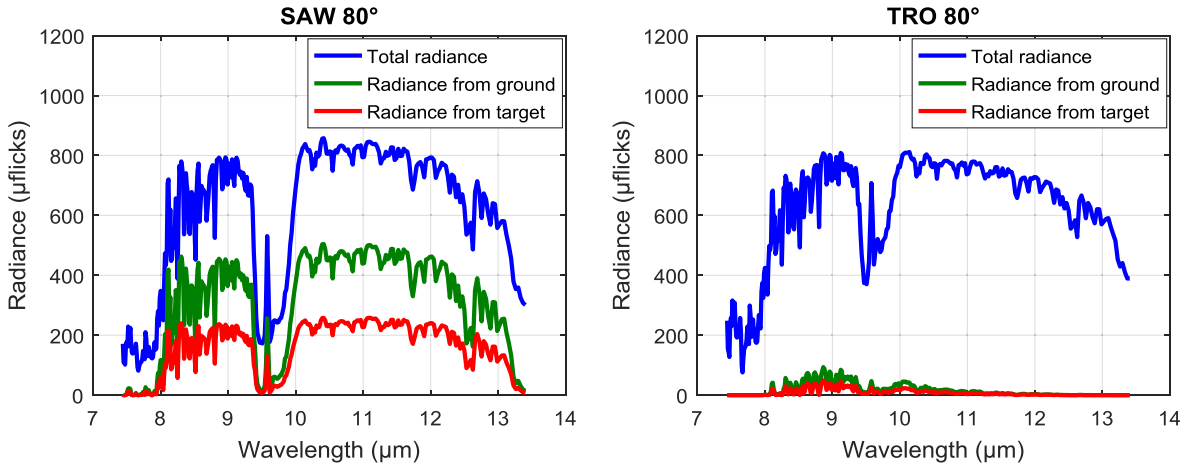

Figure 17: Radiance at aperture for two atmospheres.

Model Predictions

Figure 18 illustrates the SNR and NESR for the Concept LWIR System operating at 200 Hz frame rate. The SNR curves behave as expected due to the transmittance results above. Note that the SNR reduction from an off-nadir angle of 65° to 80° is also due to the target size (the same physical target size was used for both off-nadir angles, so it appears smaller at the longer slant range of the 80° cases). On the other hand, the NESR (at the aperture) is roughly equal for all cases. While the NESR at aperture is typically the primary KPP for LWIR HSI systems, it does not reflect the variation in performance across the different cases here.

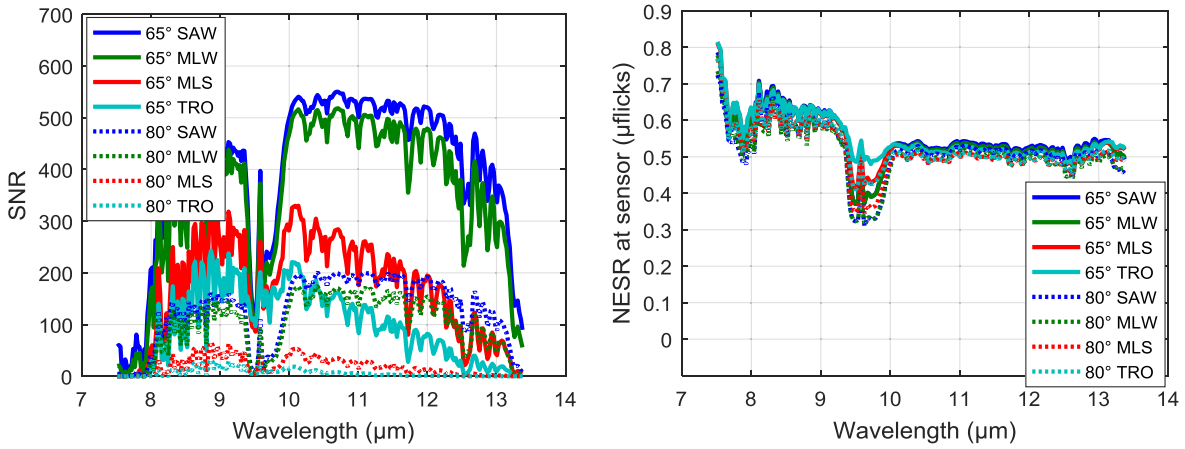

Figure 18: SNR and NESR of Concept LWIR System in Scenario 2

Another way to look at NESR is by quantifying the NESR at the target, rather than at the aperture. The NESR at the target is the NESR at the aperture divided by the transmittance of the atmospheric path. In other words, the NESR is referred to the target rather than the aperture. Figure 19 illustrates the NESR at the target. This NESR reflects the effect of atmospheric transmittance. Table 2 summarizes the performance of the Concept LWIR System at a wavelength of 10 µm.

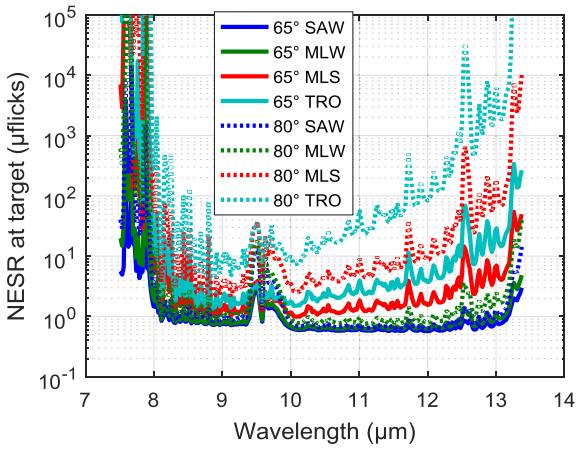

Figure 19: NESR at the target of the Concept LWIR System in Scenario 2

Table 2: LWIR Model Results, Scenario 2

Parameters	Scenario 2 (50,000ft; Sensor System Performance Results)			
CONOPS	80° Off Nadir; 200Hz; 1 co-adds; 50m/s Back Scan	80° Off Nadir; 100Hz; 1 co-adds; 50m/s Back Scan	65° Off Nadir; 200Hz; 1 co-adds; 50m/s Back Scan	65° Off Nadir; 100Hz; 1 co-adds; 50m/s Back Scan
Parameters	**Tropical Performance Results**			
$NESR_{(@10um\ in\ MLW/SB)}^{\#}$ (uf)	0.50	0.34	0.53	0.36
$SNR_{(@\ 10um\ in\ MLW/SB)}^{\#}$	14	20	188	274
Parameters	**Mid Latitude Summer Performance Results**			
$NESR_{(@10um\ in\ SAW/SB)}^{\#}$ (uf)	0.48	0.33	0.52	0.35
$SNR_{(@\ 10um\ in\ SAW/SB)}^{\#}$	38	56	282	412
Parameters	**Mid Latitude Winter Performance Results**			
$NESR_{(@10um\ in\ MLW/SB)}^{\#}$ (uf)	0.47	0.32	0.51	0.35
$SNR_{(@\ 10um\ in\ MLW/SB)}^{\#}$	135	199	466	682
Parameters	**Sub Arctic Winter Performance Results**			
$NESR_{(@10um\ in\ SAW/SB)}^{\#}$ (uf)	0.48	0.32	0.52	0.35
$SNR_{(@\ 10um\ in\ SAW/SB)}^{\#}$	160	236	497	727

DISCUSSION

It is observed from the Model results that one can achieve better system performance when imaging through long atmospheric paths by improving the overall imaging system. Increasing spectrometer transmission efficiency and that of each of its optical components directly results in an overall improvement in total system performance. This can be accomplished by decreasing the number of optical interfaces and transmission loss at each surface, or by increasing the overall spectrometer efficiency by improving the transmission efficiency of the internal optics (specifically the grating).

Another improvement is to increase the optical throughput of the system. This requires increasing either the telescope aperture or pixel size. For example, increasing the telescope aperture positively affects performance by decreasing NESR even though N_{tot} increases. Also, increasing pixel size improves performance by lowering NESR, however with increased N_{tot}. Another option to increase optical throughput is to decrease EFL which enlarges the Instantaneous Field of View, the Swath and AΩ leading to an overall reduction in the NESR. However, this leads to a growth in optical point spread function (OPSF) and an increase in GRD. These results

indicate that trades should be performed between system performance requirements and atmospheric conditions against mission needs.

Modifications to the slit width or the spectral resolution can affect the dispersion of the system. Opening the slit width decreases spectral resolution similar to spatial resolution. For gases and materials with sharp features this could decrease performance just like blurring the image can decrease spatial resolution. However, for materials with broad features like solids this will likely increase performance. Thus optical throughput and spectral resolution trades should also be performed against mission CONOPS for specific atmospheric conditions and targets.

For sub-pixel Targets the SNR metric alone does not fully address the detectability of the target. There are many target-background combinations that have the same radiance over the wavelength range that can be detected anywhere. Also, there are some target-background combinations that are very different in radiance but the target is not detectable for any condition. To assist in target detectability especially through large atmospheric volumes, an additional metric of Signal-to-Clutter (SCR) should be investigated.

The SCR metric depends on the spectral shape differences of target and background, which is a more realistic situation for target detection through large atmospheric volumes. However, the SCR is not the end all solution to determining if a collection system can detect and identify a target. It provides a metric well-known to the exploitation community that begins to address spectral contrast rather than just radiance level of a target and background. Therefore for long stand-off large off-nadir targets in highly cluttered scenes which include the atmosphere, it may be best for physics-based models to include the SCR metric to help understand and determine if a collection system can detect and identify a target. This SCR metric was presented in [9, 13].

Another factor affecting missions that require long stand-off large off-nadir collections that should be included in the atmosphere conditions is the atmospheric turbulence. Dr. Yogesh Wadadekar's talk at the course "Astro Technology I" in 2010 discussed the effects of atmospheric turbulence in Atmospheric Seeing [16]. Further investigation will be continued in this area to help improve the Model.

CONCLUSIONS

This paper presents initial results of the atmospheric effects on long stand-off airborne HSI systems operating in the reflective and emissive spectrum and used at mid-altitudes. The Model focused on the atmospheric conditions, CONOPS and the imaging System for two scenarios of a 50% reflectivity target and an olive green target in mixed background. The initial results showed that MLW and SAW were the best conditions for mission operations. From Scenario 2, the Model results showed it is possible to achieve NESR less than 12μf and SNR greater than 380 with a COTS-like NIR/SWIR Concept System.

The primary result of the LWIR study is that water vapor significantly reduces HSI performance at long slant ranges. This is an important consideration when predicting LWIR HSI system performance for standoff missions. The implication of this result is that a standoff LWIR HSI system would need to be designed and optimized specifically to operate in atmospheres with high moisture content. The difference between NESR at sensor and NESR at target is related to this phenomenon; future work will explore this area more fully. Additional work is currently being performed to better describe and understand the complex target-background configuration and the atmospheric turbulence and differential refraction influences on large off-nadir airborne HSI missions.

ACKNOWLEDGEMENTS

The Authors would like to acknowledge the Raytheon Spectral Science Team of: Randall Zywicki, Joel Buckley, Jefferson Yu, and TJ Ross.

REFERENCES

[1] Green, R. O., editor, “Special issues on imaging spectroscopy”, Remote Sensing of Environment, 65(3) (1998).

[2] Blechinger, F. et al., “HYDICE System, implementation, and performance”, Proc. SPIE 2480, 258-267 (1995).

[3] Blechinger, F. et al., “Optical concepts for high resolution imaging spectrometers”, Proc. SPIE 2480 165-179, (1995).

[4] Hackwell, J. A. et al., “LWIR/MWIR Imaging Hyperspectral Sensor for Airborne and Ground-Based Remote Sensing”, Proc. SPIE 2819, 102-107 (1996).

[5] Kerekes, J. P., et al., “Modeling of LWIR Hyperspectral System Performance for Surface Object and Effluent Detection Applications”, Proc. SPIE 4381, 348-359 (2001).

[6] Kerekes, J. P., “Full-Spectrum Spectral Imaging System Analytical Model”, IEEE Transactions on Geoscience and Remote Sensing, 43(3), 571-580 (2005).

[7] Kerekes, J. P. et al., “Spectral imaging system analytical model for subpixel objective detection”, IEEE Transactions on Geoscience and Remote Sensing, 40(5), 0881-1101 (2002).

[8] Kerekes, J. P. et al., “An analytical model of earth-observational remote sensing systems”, IEEE Transactions on Systems, Man, and Cybernetics, 21(1), 125-133 (1991).

[9] Cropper A. D. et al., “Long stand-off Performance Modelling of HSI Airborne Imaging Systems”, Proc. MSS, (2014)

[10] Shetler, B. V. et al., “Comprehensive Hyperspectral System Simulation: 1. Integrated Sensor Scene Modeling and the Simulation Architecture” Proc. SPIE 4049, 94-104 (2000).

[11] Schott, J. R. [Remote Sensing: The Imaging Chain Approach], Oxford University Press, New York, (1997).

[12] Eismann, M. T., [Hyperspectral Remote Sensing], SPIE Press, ISBN 978-0-8194-8787-2, Chapter 6,7, pp. 253-362, (2012).

[13] Cropper A. D. et al., “System-Level Performance Modeling for Next-Generation Dual-Band HSI Sensors”, Proc. MSS, (2016)

[14] Kneizys, F. X. et al., "The MODTRAN 2/3 Report and LOWTRAN 7 MODEL," Phillips Laboratory, Geophysics Directorate, Hanscom AFB (1996).

[15] Baldridge, A., et al., "The ASTER Spectral Library Version 2.0," Remote Sensing of Environment, 113, 711-715 (2009).

[16] Wadadekar, Y., “The Physics of Astronomical Seeing”, Astro Technology I (2010).